GENIORS

Research and Innovation Action (RIA)

This project has received funding from the European Union's Horizon 2020 research and innovation programme under grant agreement No 755171.

Start date : 2017-06-01 Duration : 48 Months
http://geniors.eu/

Understanding the evolution of an interface during dissolution of actinide oxide materials by macro/microscopic approaches combination

Authors : Mrs. Nicolas DACHEUX (CEA), Laurent Claparede (UM), Morgan Zunino (CNRS), Malvina Massonnet (CEA), Thomas Barral (CEA), Stephanie Szenknect (CEA), Renaud Podor (CNRS), Nicolas Dacheux (UM)

GENIORS - Contract Number: 755171

Project officer: Roger Garbil

Document title	Understanding the evolution of an interface during dissolution of actinide oxide materials by macro/microscopic approaches combination
Author(s)	Mrs. Nicolas DACHEUX, Laurent Claparede (UM), Morgan Zunino (CNRS), Malvina Massonnet (CEA), Thomas Barral (CEA), Stephanie Szenknect (CEA), Renaud Podor (CNRS), Nicolas Dacheux (UM)
Number of pages	28
Document type	Deliverable
Work Package	WP4
Document number	D4.1
Issued by	CEA
Date of completion	2021-02-03 21:41:20
Dissemination level	Error (13) !

Summary

In order to study the dissolution of uranium -lanthanide oxide solid solutions, complementary routes of preparation of precursors have been developed to prepare a large panel of solid solutions (deliverable D 4.4.). Several types of powdered and sintered samples were submitted to various dissolution tests and then the impact of several parameters of interest were evidenced. For homogeneous (U,Ce)O2 samples, uranium and cerium were released almost congruently during all the dissolution tests. Moreover, at room temperature, the evolution of all the normalized mass losses exhibited a two-steps evolution. The first one (not-catalyzed domain) was mainly associated to surface driving reactions. During the second step (catalyzed domain), the evolutions of the standardized mass losses then became non linear and corresponded to the fast release of the cations in the solution. At room temperature, the normalized dissolution rates obtained for uranium-lanthanide solid solutions were found to be higher than for the pure end members. Almost no variation versus the chemical composition was noted for x between 0.1 and 0.5 then a decrease of the normalized dissolution rate was observed for x superior to 0.5 (perhaps associated to the prevention of uranium (IV) from strong oxidation, due to large amounts of cerium in the materials). When making the dissolution tests at higher temperature (i.e. 60°C), the first step was not observed anymore (very short induction period observed). At this temperature, the dissolution of the materials remained congruent and was complete after less than 15 minutes, with a decrease of the normalized dissolution rates when incorporating lanthanide elements in the materials (possibly associated to the presence of uranium (V) in the samples). In order to study the dissolution of U1-xCexO2 solid solutions in the catalytic domain, the production of HNO2 was followed in solution. It was found that, contrarily to pure UO2, the concentration of nitrous acid was slightly lower than that of uranium, which could underline the potential consumption of HNO2 by cerium (IV). For heterogeneous sintered samples, the dissolution became uncongruent, with the preferential release of cerium compared to uranium, surely due to the presence of cerium (III) in the prepared pellets. Simultaneously, the chemical durability of the samples was decreased compared to that of homogeneous samples. Additionally, the duration of the induction period was shortened and then the ...

Approval

Date	By
2021-02-03 21:43:45	Mrs. Nicolas DACHEUX (CEA)
2021-02-04 10:34:18	Mr. Andreas GEIST (KIT)
2021-02-09 07:37:20	Mr. Stéphane BOURG (CEA)

GENIORS

GEN IV integrated oxide fuels recycling strategies

DELIVRABLE D4.1. Understanding the evolution of an interface during dissolution of actinide oxide materials by macro/microscopic approaches combination

Author(s): Laurent Claparede, Morgan Zunino, Malvina Massonnet, Thomas Barral, Stéphanie Szenknect, Nicolas Clavier, Renaud Podor, Nicolas Dacheux

Version: 1 issued on 31/01/2021

CONTENT

This project has received funding from the EURATOM research and training programme 2017-2021 under grant agreement No 755171

EXECUTIVE SUMMARY

The deliverable D4.1. *Understanding the evolution of an interface during dissolution of actinide oxide materials by macro-/microscopic approaches combination* deals with the study of the dissolution of several uranium lanthanide oxide solid solutions by using a dual approach (Task 4.1.). This task is strongly connected to Task 4.2. in which the optimization of the synthesis of various uranium bearing oxide solid solutions will be develop to prepare a large panel of materials to be submitted to dissolution tests (see deliverable D4.4. *Impact of the precursor "history" (nature, structural, microstructural and morphological parameters) during the conversion and sintering to actinide based dioxide materials*).

INTRODUCTION

The recycling of uranium, plutonium and potentially minor actinides is an important aspect to consider in order the preserve natural fissile resources and to reduce the long-term radiotoxicity of the high level radioactive waste during their final storage in a deep underground repository. Such reprocessing process involves the overall understanding of the dissolution of spent nuclear fuels, which constitutes the first step prior making the separation of all the elements of interest. This deliverable aims at contributing to the global understanding using a macro-/micro- dual approach of the materials dissolution. In this field, the dissolution of a large panel of uranium-lanthanide based oxides is examined using multiparametric dissolution tests in order to underline the effects of several parameters such as the chemical composition of the solid solution, the microstructure of the materials and the nature of the starting precursor or operating temperature on the normalized dissolution rates in concentrated nitric acid media. Secondly, operando monitoring of the solid-liquid interfaces is performed in order to follow the consequences of the dissolution on the materials microstructure (and thus their evolving reactivity) at the microscopic level. Combining both aspects will help to better understand the mechanisms involved during the dissolution of this kind of solid solutions.

MAIN RESULTS

INTRODUCTION TO THE DISSOLUTION OF URANIUM BASED CERAMICS

DESIGN OF THE DISSOLUTION EXPERIMENTS

In order to develop the multiparametric dissolution tests, the preparation then the characterization of various uranium-cerium, uranium neodymium or uranum-gadolinium solid solutions has begun in 2018. The first dissolution experiments on $(U,Ce)O_2$, $(U,Nd)O_2$ and $(U,Gd)O_2$ solid solutions have been launched in May 2018 then have been continued until now.

In order to study the impact of the several parameters of interest on the chemical durability of $U_{1-x}Ln_xO_2$ solid solutions (Ln = Ce, Nd, Gd), dissolution experiments were carried out under static conditions. Around 100 to 200 mg of powder or sintered samples were put in contact with 20 mL of 2M HNO_3 at room temperature for few days in high-density polytetrafluroethylene

This project has received funding from the EURATOM research and training programme 2017-2021 under grant agreement No 755171

(PTFE) vessels (volume of 25 mL) that avoided any adsorption of released elements on the walls of the containers. During this time, aliquots of 300 µL were regularly taken off then replaced by the same volume of fresh nitric acid solution to maintain a constant volume of solution. Depending on the dissolution conditions, i.e. on the basis of the concentration of released uranium, the aliquots were diluted with 0.2 M HNO_3 and then finally analysed by ICP-AES. The evolution of the released elements were all followed, allowing the determination of various important data, such as the normalized weight losses and associated normalized dissolution rates.

DEFINITION OF THE NORMALIZED WEIGHT LOSS AND OF THE NORMALIZED DISSOLUTION RATE

The progress of the dissolution of a solid phase (including ceramics like spent nuclear fuels) can be monitored through the determination of the normalized mass loss $N_L(i,t)$ (expressed in $g.m^{-2}$), which is defined as:

$$N_L(i,t) = \frac{m_i(t)}{f_i \times S} \quad \textbf{(1)}$$

where, $m_i(t)$ (g) is the mass of element *i* measured in solution at a given time t, S (m^2) corresponds to the surface area of the solid in contact with the solution, and f_i ($g.g^{-1}$) is the mass ratio of the element *i* in the solid. In this expression, the surface area of the sample in contact with the solution can be calculated as follows:

$$S = S_{SA} \times m_0 \quad \textbf{(2)}$$

where S_{SA} ($m^2.g^{-1}$) denotes the initial specific surface area of the solid measured by BET method, and m_0 (g) corresponds to the initial mass of solid introduced in the system.

The normalized dissolution rate, $R_L(i)$ (expressed in $g.m^{-2}.d^{-1}$), is defined as the time-derivative of the normalized mass loss, *i.e.*:

$$R_L(i) = \frac{\mathrm{d}\, N_L(i)}{\mathrm{d}t} = \frac{1}{f_i \times S} \times \frac{\mathrm{d}\, m_i}{\mathrm{d}t} \quad \textbf{(3)}$$

The use of **Equation 3** can be considered to be acceptable as soon as the surface area and the mass fraction of the element remained almost constant during the dissolution tests. On the contrary, when important variations are noted either for the reactive surface area or mass fractions, additional data, such as ratio of dissolved materials can be included in the overall analysis of the material dissolution. The dissolution is usually qualified as congruent when the normalized dissolution rate values calculated from all the elemental concentrations determined in the solution are not significantly different considering the experimental error. For a congruent dissolution, the $R_L(i)$ values determined from the release of each constitutive element in solution are then directly connected (i.e. equal) to the overall dissolution rate of the solid.

This project has received funding from the EURATOM research and training programme 2017-2021 under grant agreement No 755171

DISSOLUTION OF URANIUM AND LANTHANIDE OXIDE POWDERED SAMPLES : MACROSCOPIC APPROACH

DISSOLUTION OF $(U,CE)O_2$ SOLID SOLUTIONS

DISSOLUTION OF POWDERED SAMPLES

The study of the dissolution of uranium-lanthanide based ceramics has been conducted first on various $(U,Ce)O_2$ solid solutions. The evolution of normalized mass losses of uranium enriched samples $U_{1-x}Ce_xO_2$ (with x = 0, 0.1, 0.25 and 0.5) is presented in **Figure 1**. First, it is important to note that uranium and cerium were associated to the same behavior for each sample. Indeed, the different evolutions of the normalized mass loss exhibited a similar trend with a two-stages evolution. The first stage, that occurred before the points surrounded in blue in the dissolution curves, was associated to uncatalyzed dissolution mechanism.

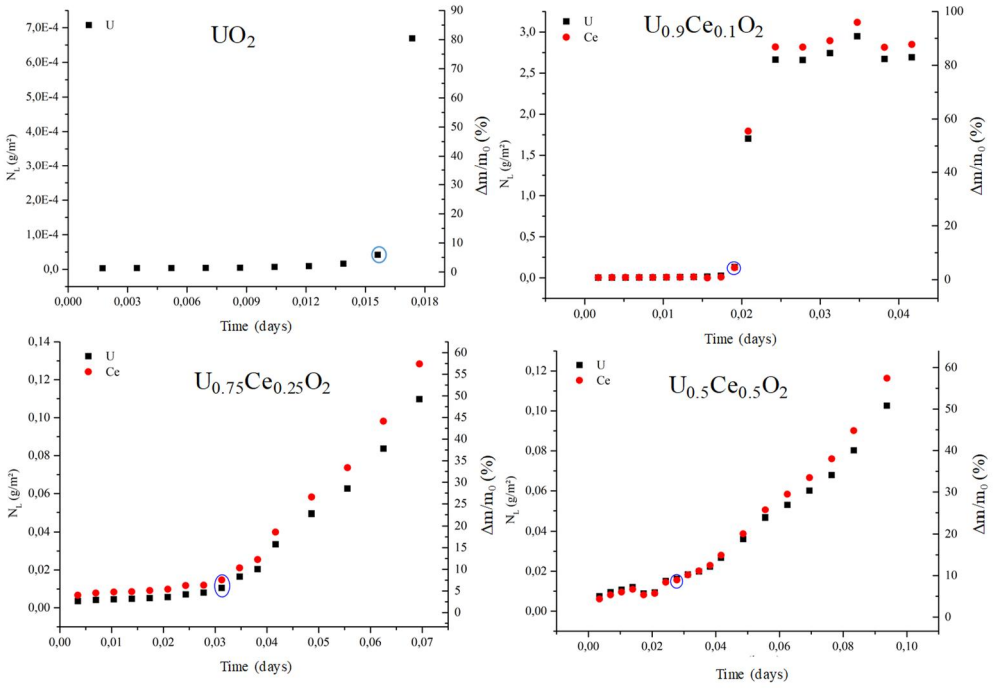

Figure 1. Evolution of the normalized weight losses $N_L(U)$ and $N_L(Ce)$ observed during the dissolution of $U_{1-x}Ce_xO_2$ (x = 0, 0.1, 0.25 and 0.5) in 2 $mol.L^{-1}$ HNO_3 at room temperature.

The dissolution rates were then driven by surface controlling reactions. During the second stage, the dissolution was controlled by catalyzed mechanisms: the evolution of the standardized mass loss then became nonlinear and corresponded to the fast release of cations in solution. These phenomena were previously observed by T. Cordara during the dissolution of UO_2 sintered samples [1]. Additionally, T. Dalger showed that the main catalytic species involved during this strong increase was (or linked to) the nitrous acid formed during the oxidation of U (IV) by nitric acid [2].

This project has received funding from the EURATOM research and training programme 2017-2021 under grant agreement No 755171

$$UO_2(s) + HNO_3(aq) + 2H^+ \rightarrow UO_2^{2+}(aq) + HNO_2(aq) + H_2O \quad \textbf{(4)}$$

The surface evolution being limited for powdered samples (compared to sintered samples), the dissolution studied was probably mainly catalyzed by the presence of nitrous acid. For the samples enriched in uranium, the dissolution seemed to have the same behavior than UO_2, uranium oxidation controlling the dissolution kinetics. In addition, the release of uranium and cerium in solution seemed to be faster when the uranium mole loading increased. However, regarding the general shape of the curves, the incorporation rate of cerium did not impact significantly the dissolution (as long as the cerium content was not higher than 50 mol.%).

The evolution of the mass losses obtained for cerium-rich compounds (i.e. for x = 1, 0.9 and 0.75) is reported in **Figure 2**. For these compounds, the solid solutions exhibited a similar behaviour with an initial pulse of uranium (about 15%). This pulse could result from several phenomena that could occur simultaneously. Firstly, uranium (IV) could be partly oxidized to uranium (VI) and consequently could be released more rapidly in solution as the uranyl form. Secondly, a less durable uranium enriched phase could be present at the surface of the sample and could be dissolved more quickly than the bulk material. This hypothesis was supported by EDS analyses, which showed spread distributions or even two closed but distinct populations for these cerium enriched compositions. However, the establishment of uncatalyzed mechanisms was observed after this first step, with a continuous increase of the normalized mass losses. The same surface reactions (adsorption and desorption of species at the solid-solution interface) were already reported by D. Horlait [3] and L. Claparede [4] when studying the dissolution of the strongly refractory CeO_2 ceramic.

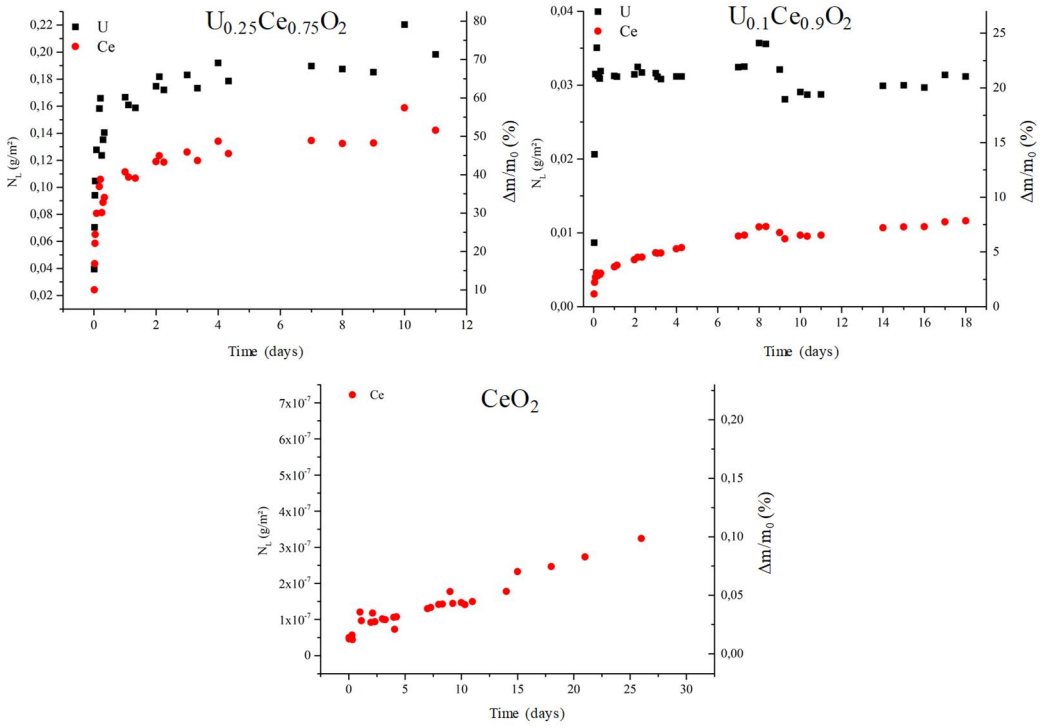

Figure 2. Evolution of the normalized weight losses $N_L(U)$ and $N_L(Ce)$ observed during the dissolution of $U_{1-x}Ce_xO_2$ (x = 0.75, 0.9 and 1) in 2 mol.L^{-1} HNO_3 at room temperature.

This project has received funding from the EURATOM research and training programme 2017-2021 under grant agreement No 755171

For each dissolution test, the normalized dissolution rates associated to each element were determined by considering the slope of the dissolution curves during the induction period. The variation of the logarithm of the normalised dissolution rate is reported as a function of the composition in **Figure 3**. Most of the dissolution tests led to congruency between uranium and cerium. Only the solid solution $U_{0.9}Ce_{0.1}O_2$ seemed to dissolve incongruently, due to the cationic heterogeneity observed for this sample. On the other hand, **Figure 2** shows that the normalized dissolution rates were very close for uranium enriched mixed oxides (x = 0.1, 0.25, 0.5). However, uranium dioxide was associated to a normalized dissolution rate of 5×10^{-4} $g.m^{-2}.d^{-1}$, lower than that obtained for the other materials. This could result from its better crystallization state compared to uranium-cerium dioxide solid solutions. For cerium enriched samples (x = 0.75, 0.9 and 1), the normalized dissolution rates decreased sharply with the increase of the cerium mole loading. These observations are in agreement with literature [3, 4] since CeO_2 (as ThO_2) exhibits stronger chemical durability than the uranium end-member, which agrees well with its refractory nature even in oxidative conditions. Moreover, for uranium enriched solid solutions, the increase of cerium mole loading only slightly affected the normalized dissolution rates.

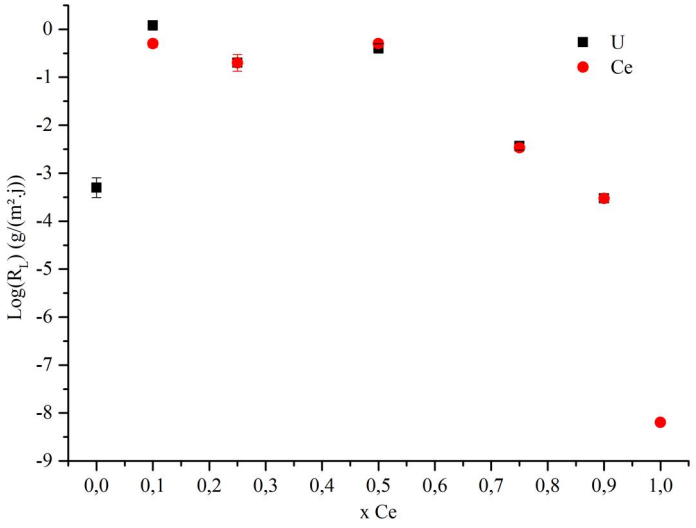

Figure 3. Variation of the logarithm of the normalized dissolution rate of $U_{1-x}Ce_xO_2$ solid solutions as a function of the cerium mole loading.

DISSOLUTION OF $U_{0.75}CE_{0.25}O_2$ SINTERED SAMPLES

The second part of the dissolution study dealt with the multiparametric study of the dissolution of $U_{0.75}Ce_{0.25}O_2$ sintered samples (relative density around 90%, see the forthcoming D4.4. deliverable) with a particular interest to the influence of HNO_3 and HNO_2 on the dissolution kinetics. First, the uncatalyzed regime was studied by varying the nitric acid concentration.

The dissolution experiments were carried out at room temperature for various concentrations of nitric acid (0.1 – 0.5 – 1 – 2 – 3 – 4 $mol.L^{-1}$ HNO_3). Depending on the dissolution rates of the samples, the experiments were carried out under static conditions (for experiments performed in 0.1 - 0.5 - 1 - 2 $mol.L^{-1}$ HNO_3) or dynamic conditions (for experiments performed in 3 - 4 $mol.L^{-1}$ HNO_3). The variation of the nitric acid concentration allowed to highlight and to quantify the impact of the redox reactions on the normalized dissolution rate. The changes in the

This project has received funding from the EURATOM research and training programme 2017-2021 under grant agreement No 755171

normalized mass loss, $N_L(i)$, and in the relative mass loss, $\Delta m/m_0$ (%), observed during the dissolution of $U_{0.75}Ce_{0.25}O_2$ sintered samples are presented in **Figure 4**.

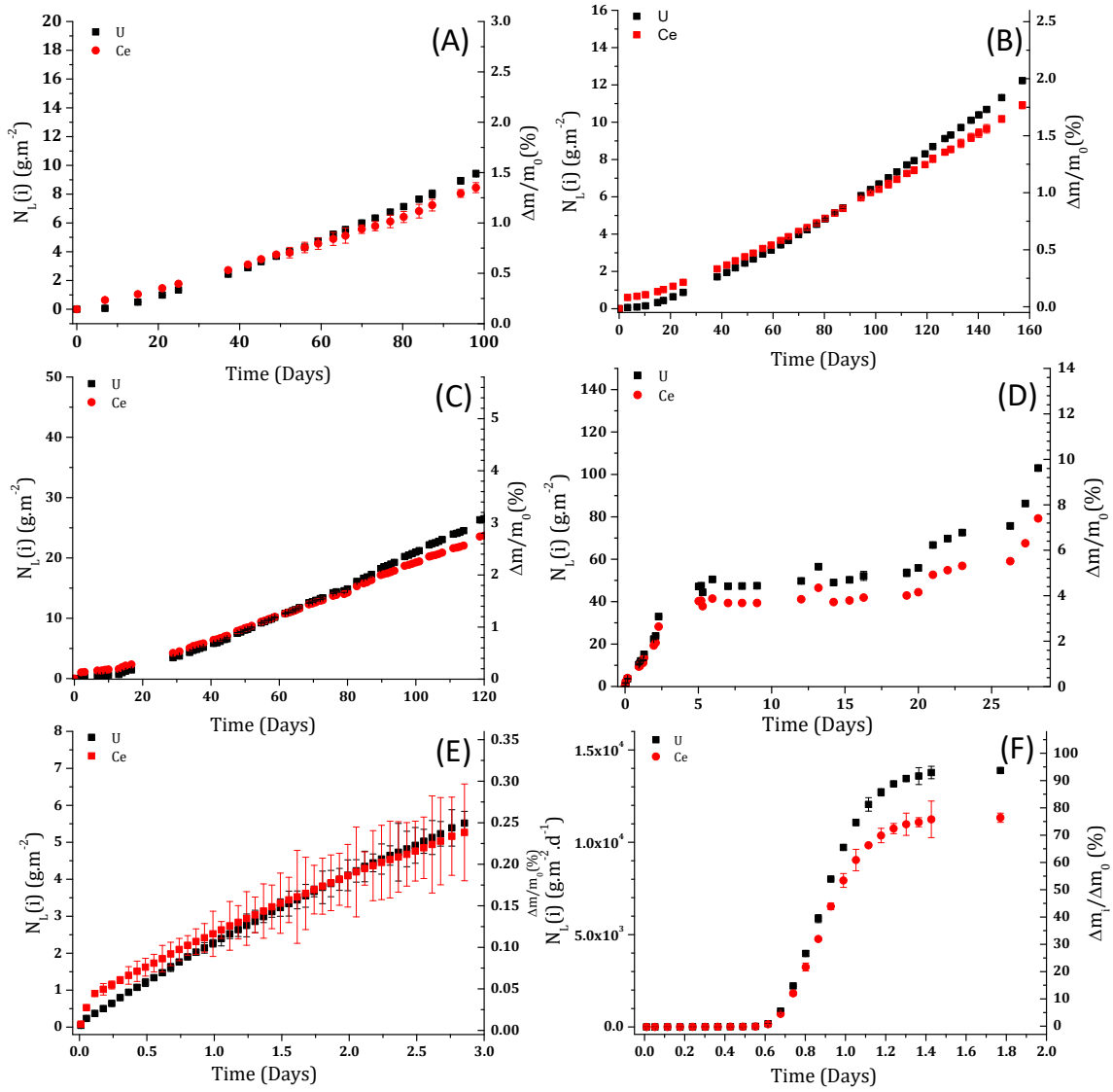

Figure 4. Evolution of the normalized mass losses and of the relative mass losses obtained during the dissolution of sintered samples of $U_{0.75}Ce_{0.25}O_2$ in 0.1 mol.L^{-1} (A), 0.5 mol.L^{-1} (B), 1 mol.L^{-1} (C), 2 mol.L^{-1} (D), 3 mol.L^{-1} (E) and 4 mol.L^{-1} (F) HNO_3.

The results obtained during the dissolution of such sintered materials exhibited several similarities with those observed for sintered UO_2 [1]. Indeed, no initial pulse was observed on the dissolution curves. The second stage, characterized by the linear evolution of mass losses and associated to the uncatalyzed regime, was however observed during all the experiments. Thus, the normalized dissolution rates R_L were determined during this step.

The catalysed regime (step 3) could be only observed during dissolution tests performed in 4 mol.L^{-1} HNO_3. It therefore appeared that the conditions for accessing the catalysed regime were more difficult to reach for $U_{0.75}Ce_{0.25}O_2$ than for $U_{0.75}Th_{0.25}O_2$ [2]. Indeed, the permanent

This project has received funding from the EURATOM research and training programme 2017-2021 under grant agreement No 755171

regime corresponding to the second step of the dissolution was maintained until a progress of the reaction of dissolution of 3 to 4 mass.% was reached (the transition from step 2 to step 3 taking place for a relative mass loss of ≈ 2 mass.% for $Th_{0.25}U_{0.75}O_2$) [2]. Consequently, the duration of the induction period was extended when performing the dissolution of $U_{0.75}Ce_{0.25}O_2$ sintered samples.

Several papers published in the literature highlighted the predominant role of redox reactions in the mechanisms occurring during the dissolution of uranium oxide based compounds in nitric acid. In particular, the balance equations involved during the oxidative dissolution of UO_2 as well as the reduction reaction of Ce(IV) by nitrous acid are listed below.

$$UO_2(s) + HNO_3(aq) + 2H^+ \rightarrow UO_2^{2+}(aq) + HNO_2(aq) + H_2O \quad \textbf{(5)}$$

$$UO_2(s) + 2HNO_2(aq) + 2H^+ \rightarrow UO_2^{2+}(aq) + 2NO(aq) + 2H_2O \quad \textbf{(6)}$$

$$2Ce^{4+} + HNO_2 + H_2O \rightarrow 2Ce^{3+} + HNO_3 + 2H^+ \quad \textbf{(7)}$$

$$2NO(aq) + HNO_3(aq) + H_2O \rightleftarrows 3HNO_2(aq) \quad \textbf{(8)}$$

In order to complete the overall understanding of the dissolution mechanism for uranium-cerium solid solutions, the evolution of nitrous acid concentration was followed during the dissolution of $U_{0.75}Ce_{0.25}O_2$ in 4 mol.L^{-1} HNO_3 (**Figure 5**).

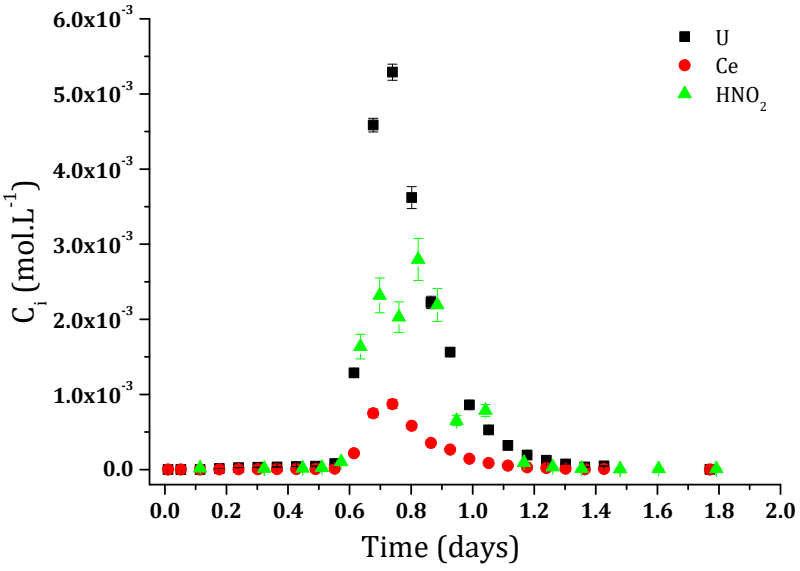

Figure 5. Evolution of uranium, cerium and nitrous acid concentrations measured during the dissolution of $U_{0.75}Ce_{0.25}O_2$ sintered pellet in 4 mol.L^{-1} HNO_3 at room temperature under dynamic conditions.

As expected, the strong production of HNO_2 occurred during the third step (i.e. during the establishment of the catalysed domain), which confirms the preponderant role of this species on the dissolution kinetics of uranium enriched samples. The variations of HNO_2 and uranium

This project has received funding from the EURATOM research and training programme 2017-2021 under grant agreement No 755171

concentrations were found to be concomitant, as it was already observed when making the dissolution of sintered UO_2. However, when uranium concentration reached a maximum value of 5.3×10^{-3} mol.L^{-1} in solution, the HNO_2 concentration did not exceed 3×10^{-3} mol.L^{-1}. Consequently, the equimolar ratio observed in solution between both concentrations when dissolving $Th_{0.25}U_{0.75}O_2$ sintered pellets [2] was not respected for $U_{0.75}Ce_{0.25}O_2$ (i.e. in the presence of cerium). Due to the instability of HNO_2 beyond 2×10^{-3} mol.L^{-1}, it was possible that a large amount of HNO_2 decomposed before the analysis. Another explanation could come from the existence of redox reaction between Ce(IV) and HNO_2 in solution (**Equation 7**), as reported in the literature. HNO_2 produced by oxidation of U(IV) into U(VI) could therefore be partly consumed by redox reaction with Ce(IV). This hypothesis can also support the extension of the induction period, which is associated to the transition from non-catalysed to catalysed domains.

Concerning the non-catalysed period, the normalized dissolution rates were determined during the second step of the dissolution curves (**Table 1**) for various nitric acid concentrations. Moreover, the determination of the congruence ratio, $r = R_L(Ce) / R_L(U)$, showed that the dissolution was always congruent, for all the dissolution conditions examined (with r values ranging from 0.7 to 1). This result also validated the homogeneity of the prepared solid solutions. The variation of the R_L values (uncatalyzed regime) versus the initial nitric acid concentration is reported in **Table 1**.

Table 1. Normalized dissolution rates R_L (i) (expressed in g.m^{-2}.d^{-1}) obtained during the dissolution of sintered samples of $U_{0.75}Ce_{0.25}O_2$ for various nitric acid concentrations. The associated relative weight losses as well as the congruence ratios $r = R_L(Ce) / R_L(U)$ are also included.

HNO_3	0.1 mol.L^{-1}	0.5 mol.L^{-1}	1 mol.L^{-1}	2 mol.L^{-1}	3 mol.L^{-1}	4 mol.L^{-1}
$R_L(U)$	$(9.3 \pm 0.1)\times10^{-3}$	$(7.7 \pm 0.2)\times10^{-3}$	0.233 ± 0.002	0.9 ± 0.2	2.0 ± 0.1	11 ± 6
$R_L(Ce)$	$(7.0 \pm 0.2)\times10^{-3}$	$(6.7 \pm 0.1)\times10^{-3}$	0.207 ± 0.002	0.7 ± 0.2	1.69 ± 0.02	10 ± 5
r	0.75 ± 0.02	0.87 ± 0.03	0.89 ± 0.01	0.7 ± 0.2	0.84 ± 0.01	1 ± 1
$\Delta m/m_0$	2 %	2 %	2 %	1.6 %	0.25 %	1.3 %
	End of step 2					

The R_L values obtained for $U_{0.75}Ce_{0.25}O_2$ sintered samples differed from those reported for UO_2 [1] or $Th_{0.25}U_{0.75}O_2$ solid solutions [2] in the same conditions. In particular, the normalized dissolution rates of $U_{0.75}Ce_{0.25}O_2$ reached $R_L = 9.3 \times 10^{-3}$ g.m^{-2}.d^{-1} in 0.1 mol.L^{-1} HNO_3. When dissolving $Th_{0.25}U_{0.75}O_2$ sintered sample in the same conditions [2], the value obtained in non-catalysed period was lower by approximately one order of magnitude (i.e. $R_L = 1.0\times 10^{-3}$ g.m^{-2}.d^{-1}). This difference was progressively hindered when increasing the acidity of the solution, to finally become negligible in 4 mol.L^{-1} HNO_3 ($R_L = 11$ g.m^{-2}.d^{-1} and $R_L = 10.26$ g.m^{-2}.d^{-1} for $U_{0.75}Ce_{0.25}O_2$ and $Th_{0.25}U_{0.75}O_2$, respectively). Also, the incorporation of cerium in uranium bearing oxides induced lower chemical durability of the samples in low concentrated nitric acid solutions (typically for $C_{HNO3} < 1$ mol.L^{-1}). These results also underlined that when increasing the nitric acid concentration, cerium incorporation led to less pronounced effect on the dissolution kinetics. Thus, the oxidation of uranium (IV) by HNO_3 therefore became the predominant mechanism, which controlled the overall kinetics of dissolution for high nitric acid concentrations. This different behaviour of $U_{0.75}Ce_{0.25}O_2$ compared to $Th_{0.25}U_{0.75}O_2$ [2] was also observed for mixed uranium oxides containing trivalent lanthanides [3]. Several hypotheses were formulated to explain such a difference.

This project has received funding from the EURATOM research and training programme 2017-2021 under grant agreement No 755171

↳ First hypothesis

Cerium (IV) was partly reduced to cerium(III) during the sintering of the pellets under reducing conditions (Ar-4%H_2). In these conditions, uranium could be was partly present as uranium (V) or uranium (VI) due to the required charge compensation. This could affect the chemical durability of the materials. Moreover, Tocino showed by EELS spectroscopy associated with TEM that the prepared $U_{0.75}Ce_{0.25}O_2$ sintered samples contained a not-negligible cerium (III) content with no uranium (V) or (VI) [6]. This result indicates that for these samples, the charge compensation was ensured by the presence of oxygen vacancies [3]. The presence of these structural defects would decrease the energy of cohesion of the material and, therefore, could affect the intrinsic chemical durability of the solid solution as it has been already demonstrated for $Th_xNd_{1-x}O_{2-x/2}$ solutions solids [5].

↳ Second hypothesis

Assuming that all cerium was present as cerium (IV), it is possible that even for low acid concentrations, cerium (IV) could react with nitrogen-based species, leading to the increase of the dissolution rates. Reductive dissolution was shown to be particularly efficient in accelerating the dissolution kinetics of highly refractory CeO_2. According to **Equation 7**, nitrous acid formed in the solution due to the reduction of nitrates could be able to reduce cerium (IV) into cerium (III). This species could be present in an amount that could not be detected in slightly concentrated nitric acid solutions. However, its local production near the solid / solution interface through redox reaction with uranium (IV) may be sufficient to develop such kind of redox reaction.

DISSOLUTION OF $U_{0.75}CE_{0.25}O_2$ SINTERED SAMPLES: IMPACT OF THE CHEMICAL HOMOGENEITY

In order to study the behaviour of heterogeneous mixed oxides, $(U,Ce)O_2$, several samples with a cerium incorporation rate of 25 and 50 mol.% have been synthesized according to **Equation 9**. Both precursors UO_2 and CeO_2 were ground together in the desired chemical ratio in a grinding jar (25 Hz for 15 minutes) using a three-dimensional oscillating mill (25 Hz for 15 minutes). The mixed oxides $U_{0.75}Ce_{0.25}O_2$ and $U_{0.5}Ce_{0.5}O_2$ thus obtained were subsequently called “mother mixtures”.

$$(1-x)\,UO_2 + x\,CeO_2 \rightarrow U_{1-x}Ce_xO_2 \qquad \textbf{(9)}$$

The obtained mixtures were then diluted with UO_2 to finally obtain model compounds with the following average compositions of $U_{0.9}Ce_{0.1}O_2$ and $U_{0.75}Ce_{0.25}O_2$ and heterogeneous cation distribution (**Equation 10**).

$$(1-y)\,UO_2 + y\,U_{(1-x')}Ce_{x'}O_2 \rightarrow U_{(1-x)}Ce_xO_2 \quad \text{with} \quad x = y \times x' \qquad \textbf{(10)}$$

From the powders obtained, pellets of 400 mg were prepared by uniaxial pressing at 500 MPa in a 8 mm diameter die. The sintering of pellets was then carried out at 1700°C for 4 hours under a reducing atmosphere (Ar – 4% H_2). SEM-EDS (Energy Dispersive Spectroscopy) maps of the surface of the raw and sintered pellets were finally carried out in order to evaluate the sample heterogeneity in terms of cationic distribution within the material. A selected area of approximately 100-150 mm^2 was analyzed for 4 hours. These conditions guaranteed reliable counting statistics associated to a large number of dots (≈ 750,000), which were considered to

This project has received funding from the EURATOM research and training programme 2017-2021 under grant agreement No 755171

be representative of the overall area of the pellets. In addition, the count rate was kept constant for all the analysed zones in order to avoid any bias in the quantification. SEM-EDS clearly highlighted the heterogeneous cationic distribution within the (U,Ce)O_2 pellets (**Figure 6** and **Figure 7**).

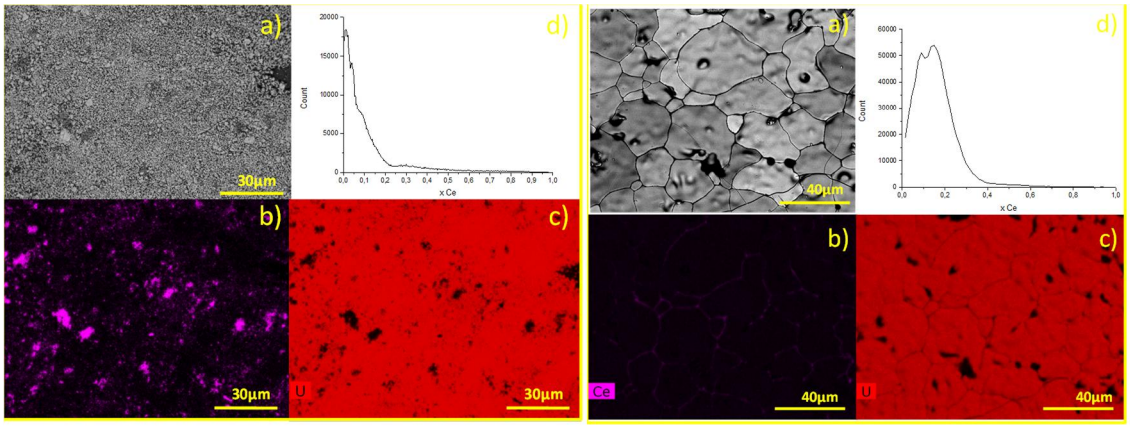

Figure 6. EDS mapping obtained for the raw powder (left) and for sintered pellet (right) of $U_{0.9}Ce_{0.1}O_2$: SEM image (a), EDS mapping for cerium (b) and uranium (c) and representation of the cation distribution (d).

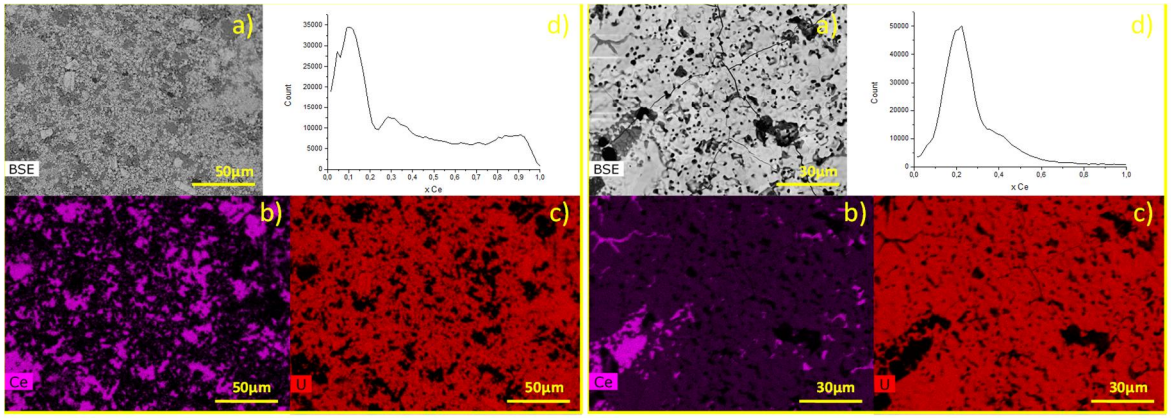

Figure 7. EDS mapping obtained for the raw powder (left) and for sintered pellet (right) of $U_{0.75}Ce_{0.25}O_2$: SEM image (a), EDS mapping for cerium (b) and uranium (c) and representation of the cation distribution (d).

EDS mapping showed that all the analyzed pellets exhibited an heterogeneous cationic distribution with the presence of cerium enriched zones surrounded by the UO_2 matrix. These enriched zones were found to form small agglomerates of 1 -10 µm in size. Nevertheless, the sintering step led to significant homogenization compared to the raw materials due to the cationic diffusion at high temperature. For $U_{0.9}Ce_{0.1}O_2$ sintered samples, the only residual cerium enriched zones were located within the grain boundaries, which suggested the partial reduction of Ce (IV) into Ce (III). Conversely, for $U_{0.75}Ce_{0.25}O_2$, the small cerium enriched initial agglomerates formed larger agglomerates of several tens of µm in size after heating. However, the absence of pure CeO_2 within the pellet may suggest that these large agglomerates were constituted by the same phase, with a gradient in composition.

This project has received funding from the EURATOM research and training programme 2017-2021 under grant agreement No 755171

Dissolution tests were carried out at room temperature on these samples in static conditions under stirring. With this aim, several fragments of the pellet (approximately 100 to 200 mg) were placed in a closed reactor containing 20 mL of 2 mol.L^{-1} HNO_3. The evolutions of the mass losses calculated from uranium and cerium amounts release in solution during dissolution tests of $U_{0.9}Ce_{0.1}O_2$ are presented in **Figure 8**.

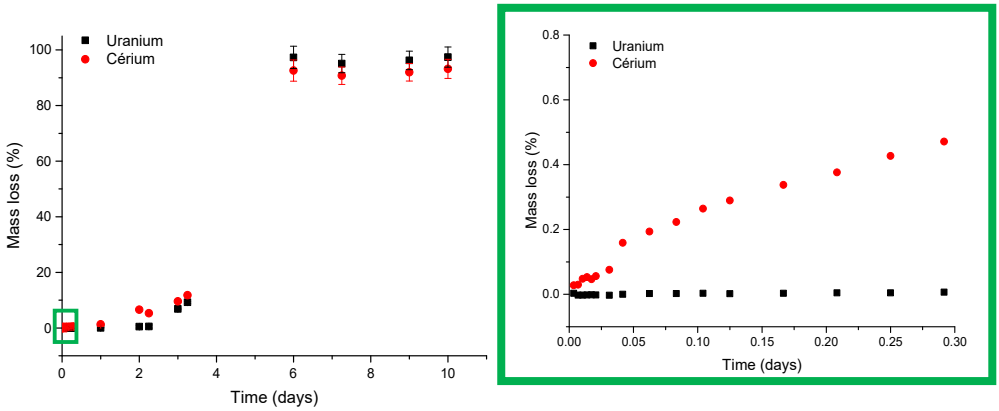

Figure 8. Evolution of the uranium and cerium relative mass losses obtained during the dissolution of heterogeneous $U_{0.9}Ce_{0.1}O_2$ sample in 2 mol.L^{-1} HNO_3 at RT.

During the first days of dissolution test, a very low uranium release was observed in solution. Conversely, cerium began to dissolve immediately to reach 0.5 wt.% of relative mass after only 7 hours of dissolution test. Dissolution was therefore found to be incongruent. This phenomenon was certainly due to the presence of cerium (III), which induces a loss in the chemical durability compared to pure cerium (IV) bearing materials. Such a trend was also confirmed for the heterogeneous $U_{0.75}Ce_{0.25}O_2$ samples (**Figure 9**). For these latter, a relative mass loss of only 0.9 wt.% was noted after 7 hours of dissolution for uranium compared to 14.1 wt.% for cerium. However, the comparison of the two samples revealed an increase of the cerium release with the cerium incorporation rate in the material in the early beginning of the dissolution

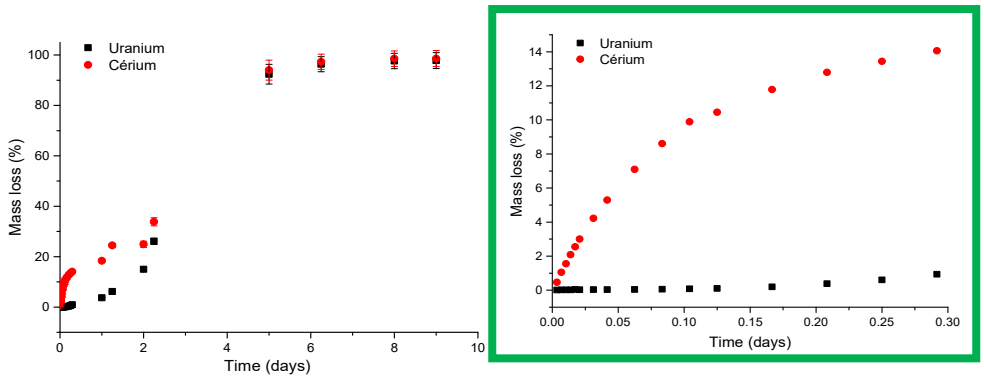

Figure 9. Evolution of the uranium and cerium relative mass losses obtained during the dissolution of heterogeneous $U_{0.75}Ce_{0.25}O_2$ sample in 2 mol.L^{-1} HNO_3 at RT.

As a summary, the cationic distribution in the material led to the decrease of the chemical durability of the pellets compared to homogeneous ceramics. Indeed, the induction period was

This project has received funding from the EURATOM research and training programme 2017-2021 under grant agreement No 755171

found to be shorter, leading to the rapid establishment of the catalyzed domain and thus to the total dissolution of the pellet in only 5 - 6 days at room temperature. Moreover, it is worth noting that the duration of the induction period was not strongly impacted by the chemical composition of the prepared solid solution.

DISSOLUTION OF SINTERED SAMPLES $U_{0.75}CE_{0.25}O_2$: IMPACT OF THE SINTERING ATMOSPHERE

In order to underline the impact of the sintering atmosphere on the chemical durability of the $U_{1-x}Ce_xO_2$ samples, several solid solutions were prepared by hydroxide precipitation [8,9] then the obtained precursors were shaped and densified under Ar and Ar-H_2 atmospheres at 1400°C for 10 hours. The two pellets exhibited densification rates close to 94%. The evolutions of the normalized mass losses and of the relative mass losses obtained during the dissolution of the samples in 2 mol.L^{-1} HNO_3 at room temperature are reported in **Figure 10**.

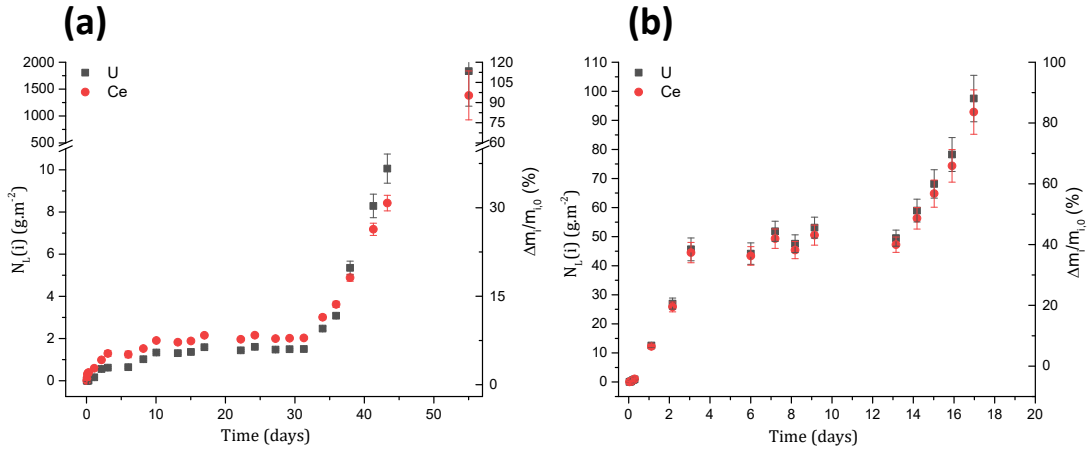

Figure 10. Evolution of the normalized mass losses and of the relative mass losses obtained during the dissolution, in 2 mol.L^{-1} HNO_3 and at room temperature, of $U_{0.74}Ce_{0.26}O_2$ samples sintered under Ar-H_2 (a) and Ar (b) atmosphere.

The dissolution appeared to be faster for the Ar-sintered pellet with complete dissolution in only 18 days, compared to the 55 days required for the pellets densified under Ar-H_2 atmosphere. However, the biggest difference came from the evolution of mass losses. Indeed, for the pellets prepared under Ar-H_2 atmosphere, the evolution of the cationic release was typical of UO_2 with an induction period (step 2) of about 30 days followed by a strong acceleration after dissolution of 7 mass.% due to surface evolution and to the presence of nitrous acid. It is also worth noting that the presence of a pulse was observed during the first 3 days of dissolution, with a preferential release of cerium (about 6%). These evolutions were totally different to that obtained for the pellets prepared under Ar atmosphere, with no induction period but a rapid release of cations, a ratio of 40 mass.% of dissolution being obtained after 4 days. Then, a plateau was observed with a very slow residual dissolution after 10 days, finally followed by a final acceleration to achieve the full dissolution of the sintered material. This

This project has received funding from the EURATOM research and training programme 2017-2021 under grant agreement No 755171

unusual 3-steps process was attributed to some important changes in the elemental speciation within the mixed oxide. Indeed, XANES studies provided on this kind of samples have shown that the pellets prepared under Ar atmosphere presented a large proportion of uranium (V) and cerium (III), which differed from the speciation observed for samples sintered under Ar-H_2, leading to the formation of mainly uranium (IV) and cerium (IV). This could explain the modification of the dissolution mechanism between both series of samples.

OPERANDO MONITORING OF THE SOLID/LIQUID INTERFACE DURING THE DISSOLUTION OF $U_{0.89}CE_{0.11}O_2$ SINTERED PELLETS BY ESEM : MICROSCOPIC APPROACH

In order to better understand the differences observed between both series of materials at the macroscopic scale, operando monitoring of the solid/liquid interface during dissolution was carried out by Environmental Scanning Electron Microscopy (ESEM). The evolution of the normalized mass losses and of the relative mass losses obtained during the dissolution of $U_{0.89}Ce_{0.11}O_2$ samples sintered under both atmospheres in 2 mol.L^{-1} HNO_3 and at room temperature are reported in **Figure 11**. The associated micrographs of the evolving surface followed by ESEM are reported in **Figure 12**.

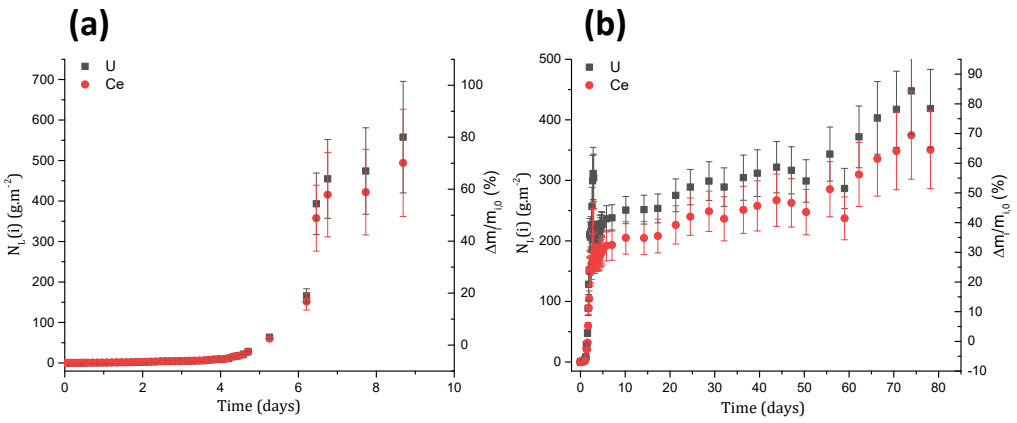

Figure 11. Evolution of the normalized mass losses and of the relative mass losses obtained during the dissolution of $U_{0.89}Ce_{0.11}O_2$ samples sintered under Ar-H_2 (a) and Ar (b) atmosphere in 2 mol.L^{-1} HNO_3 and at room temperature.

As for the $U_{0.74}Ce_{0.26}O_2$ sample, the same differences in the evolution of mass losses were observed. However, for $U_{0.89}Ce_{0.11}O_2$ solid solution densified under Ar atmosphere, even if the plateau appeared once again at about 40 mass.% dissolution (5 days of dissolution), it was found to be much longer than for $U_{0.74}Ce_{0.26}O_2$; full dissolution being not reached even after 80 days.

The monitoring of the pellets surface by ESEM first showed a significant difference in the microstructure between the two compounds, which nevertheless exhibited close densification rates (95%). In fact, the pellet prepared under Ar atmosphere was composed of grains with a 20 to 30 times larger size. This result was explained by the overstoichiometric nature of the sample due to the presence of uranium (V) and (VI) within the ceramic, which was able to

This project has received funding from the EURATOM research and training programme 2017-2021 under grant agreement No 755171

promote grain growth. However, this microstructural difference was not sufficient to explain alone the strong differences observed in the evolution of the mass losses.

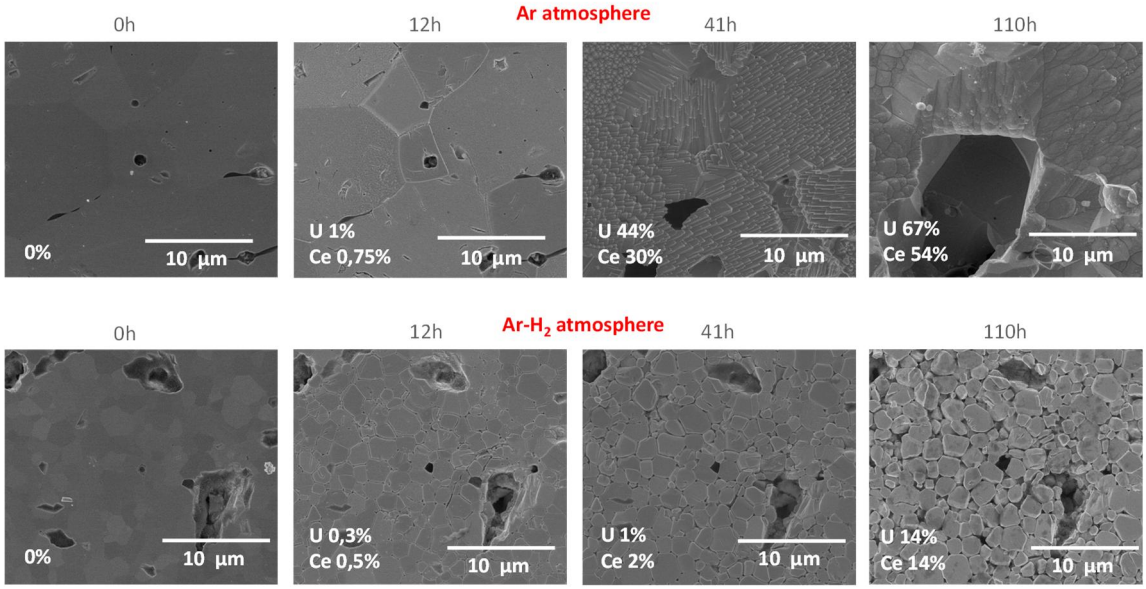

Figure 12. Results of operando monitoring by ESEM of the solid/liquid interface obtained during the dissolution of $U_{0.89}Ce_{0.11}O_2$ samples sintered under Ar-H_2 and Ar atmosphere in 2 mol.L^{-1} HNO_3 and at room temperature.

The series of ESEM micrographs clearly showed the progressive degradation of the material surface, and then suggested an increase of the reactivity of the sintered pellets in contact with the solution. The preferential dissolution of the grain boundaries was clearly observed for sintered pellets prepared under Ar-H_2 atmosphere (see the micrograph recorded after 110 hours of dissolution). This result was surely due to a small enrichment in cerium within the grain boundaries, also explaining the slight pulse observed during the first days of dissolution. This preferential attack subsequently induced the progressive pulled out of some grains at the solid/liquid interface. For the sintered samples prepared under Ar atmosphere, the microstructure degradation occurred more homogeneously, progressively revealing some crystal orientations. Here, square pyramids and chevron-type features are associated to the (100) and (110) orientation of the fluorite structure, respectively. Such an evolution induced some slight differences in the dissolution kinetics as a function of the grain orientation.

This project has received funding from the EURATOM research and training programme 2017-2021 under grant agreement No 755171

DISSOLUTION OF $(U,ND)O_2$ AND OF $(U,GD)O_2$ SOLID SOLUTIONS

DISSOLUTION OF POWDERED SAMPLES OF $(U,ND)O_2$ AND OF $(U,GD)O_2$

The same experimental protocol was applied for the dissolution of powdered $U_{1-x}Nd_xO_{2-y}$ and $U_{1-x}Gd_xO_{2-y}$ solid solutions. The dissolution tests were performed on samples with high uranium mole loading taking into account two operating temperatures: room temperature and 60°C. The results obtained for $U_{1-x}Nd_xO_{2-y}$ (x = 0.05 , 0.09 , 0.18 and 0.46) and for $U_{1-x}Gd_xO_{2-y}$ (x = 0.046 , 0.095 , 0.19 and 0.5) are presented in **Figure 13** and **Figure 14**, respectively.

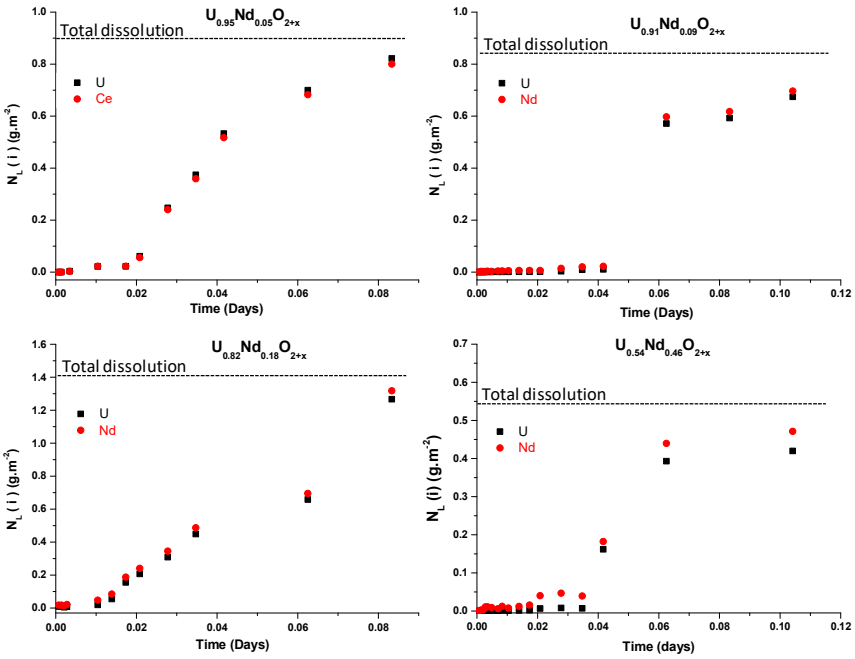

Figure 13. Evolution of the normalized weight losses $N_L(U)$ and $N_L(Nd)$ obtained during the dissolution of $U_{1-x}Nd_xO_{2-y}$ powders in 2 mol.L^{-1} HNO_3 at room temperature.

Whatever the composition and the nature of the doping element, the evolutions of the normalized mass losses $N_L(U)$, $N_L(Nd)$ and $N_L(Gd)$ were the same than that obtained for $U_{1-x}Ce_xO_2$ solid solutions (x > 0.5). Indeed, these evolutions followed the two-steps trend for all the samples. Moreover, uranium, neodymium and gadolinium were released congruently. The chemical durability was found to be close, with a full dissolution of the powder after less than 2.5 hours. The time associated to the uncatalyzed dissolution mechanisms was usually ranging from 30 minutes to 1 hour. Surely due to better crystallization state, this period was better defined and longer for compounds doped with gadolinium. The variation of the normalized dissolution rates is plotted as a function of composition in **Figure 15**. Once again, the normalized dissolution rates obtained for the solid solutions were found to be 3 orders of magnitude higher than that reported for UO_2 (**Figure 3**, i.e. 5×10^{-4} $g.m^{-2}.d^{-1}$). As suggested for $Ce_{1-x}Ln_xO_{2-x/2}$ [3] and $Th_{1-x}Ln_xO_{2-x/2}$ [5] solid solutions, such an effect could be linked to the decrease of the energy of cohesion of the crystal structure associated to the incorporation of trivalent elements (potential presence of oxygen vacancies). Moreover, a slight increase of the normalized dissolution rates was observed as a function of the gadolinium mole loading.

This project has received funding from the EURATOM research and training programme 2017-2021 under grant agreement No 755171

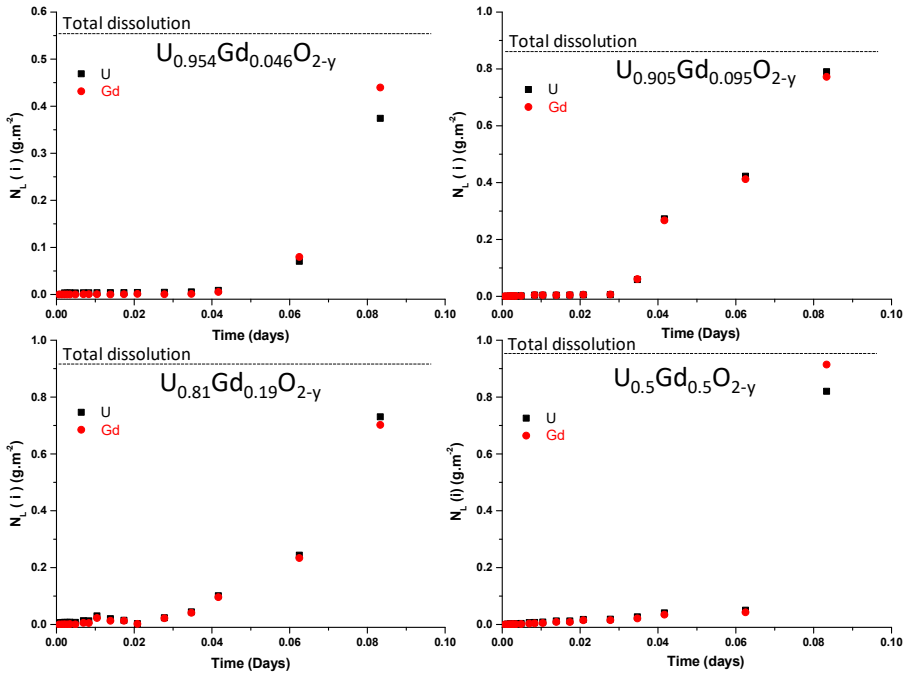

Figure 14. Evolution of normalized weight losses $N_L(U)$ and $N_L(Gd)$ observed during the dissolution of $U_{1-x}Gd_xO_{2-y}$ powders in 2 $mol.L^{-1}$ HNO_3 at room temperature.

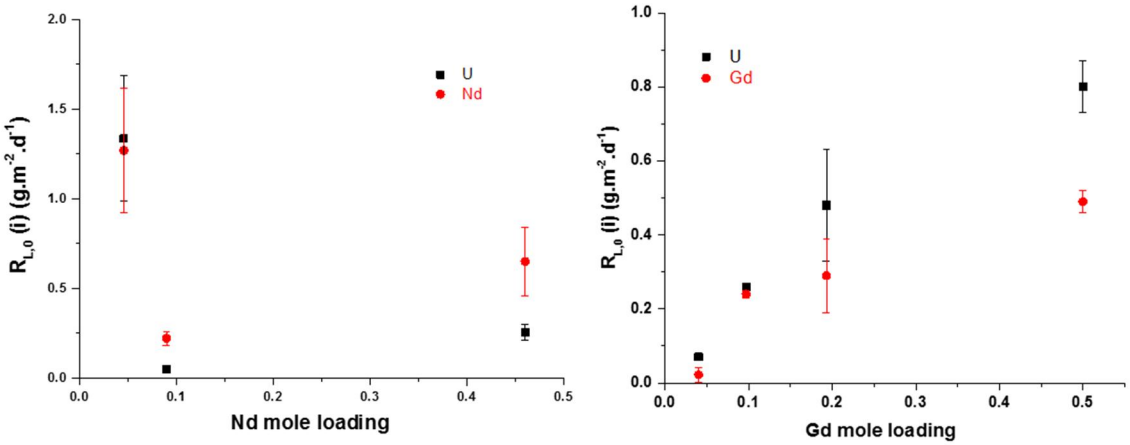

Figure 15. Variation of the normalised dissolution rate versus the neodymium and gadolinium mole loadings when performing the dissolution tests in 2 $mol.L^{-1}$ HNO_3 at room temperature.

According to the literature [1,5], the dissolution kinetics was expected to be strongly dependent on temperature. Thus, dissolution tests were also performed at 60°C in 2 $mol.L^{-1}$ HNO_3. The evolution of the normalized mass losses obtained for $U_{1-x}Nd_xO_{2-y}$ (x = 0.05 , 0.09, 0.18 and 0.46) and for $U_{1-x}Gd_xO_{2-y}$ (x = 0.046 , 0.095, 0.19 and 0.5) are presented in **Figure 16** and in **Figure 17**, respectively. As it was expected, the normalized dissolution rates widely increased with increasing temperature. More often, the full dissolution of the samples was reached for

This project has received funding from the EURATOM research and training programme 2017-2021 under grant agreement No 755171

less than 15 minutes. If the temperature did not affect the congruency of the dissolution, the general trend was clearly modified, with the disappearance of the induction period. Only the second step was evidenced, meaning that the dissolution was rapidly connected to catalyzed mechanisms at this temperature.

However, contrarily to the studies performed on sintered pellets, which revealed strong microstructural evolution with the progress of the dissolution reaction, that developed on powders showed linear evolution of the normalized mass loss. This behavior was explained by the low evolution of the reactive surface during dissolution tests for powdered samples. The normalized dissolution rates obtained during the catalytic period are plotted as a function of the composition in **Figure 18**. Compared to the previous experimental conditions, the incorporation of the trivalent elements induced a decrease by a factor of 3 of the normalized dissolution rate when comparing the results obtained for $U_{0.95}Ln_{0.05}O_{2+x}$ and $U_{0.5}Ln_{0.5}O_{2+x}$. Since the dissolution kinetics was here controlled by the rapid oxidation of uranium (IV) into uranium (VI) due to the presence of catalytic species in solution such as nitrous acid, this tendency was surely linked to the decrease of the uranium content in the solid. Moreover, the variation of the normalized dissolution rate remained rather low due to the presence of the trivalent elements which induced weakness (decrease of energy of cohesion) in the crystal structure. Thus, two antagonistic effects were existing during the catalysed-driven dissolution.

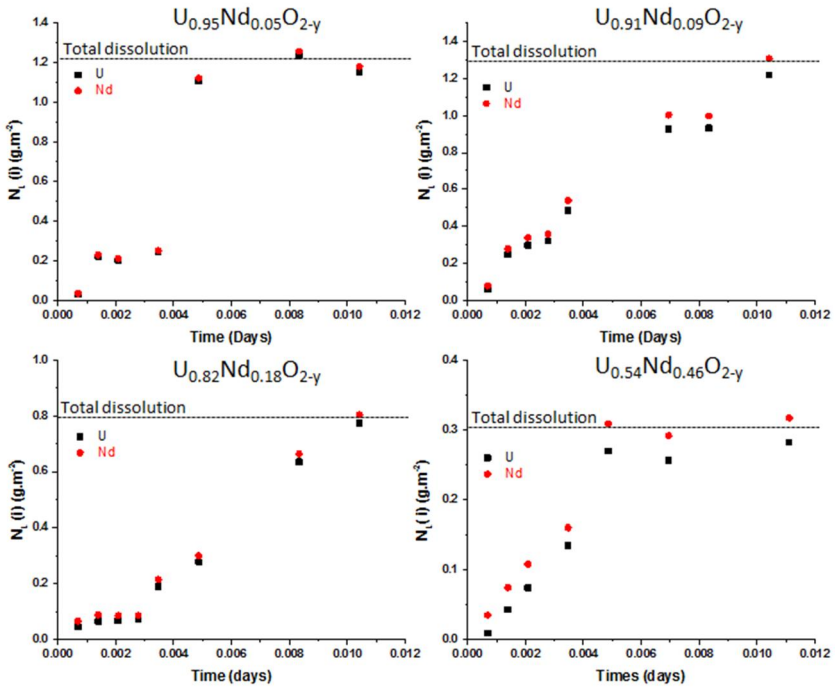

Figure 16. Evolution of normalized weight losses $N_L(U)$ and $N_L(Nd)$ obtained during the dissolution of $U_{1-x}Nd_xO_{2-y}$ in 2 mol.L^{-1} HNO_3 at 60°C.

This project has received funding from the EURATOM research and training programme 2017-2021 under grant agreement No 755171

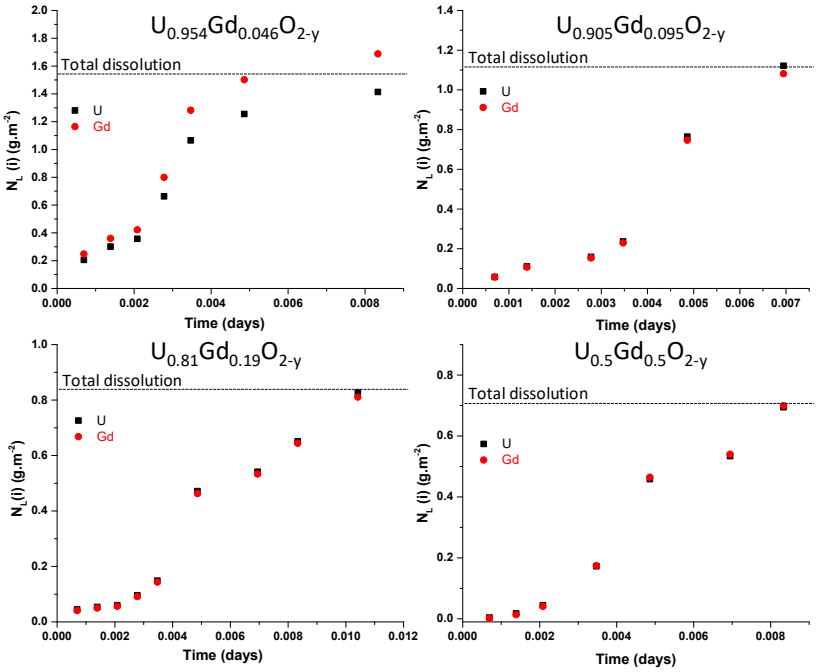

Figure 17. Evolution of normalized weight losses $N_L(U)$ and $N_L(Gd)$ obtained during the dissolution of $U_{1-x}Gd_xO_{2-y}$ in 2 mol.L^{-1} HNO_3 at 60°C.

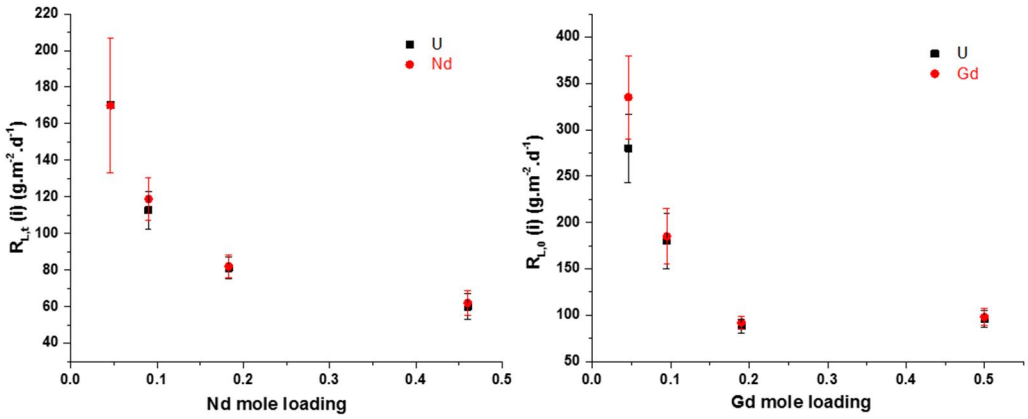

Figure 18. Variation of the normalised dissolution rate as a function of the neodymium and gadolinium mole loadings during the dissolution of $U_{1-x}Nd_xO_{2-y}$ and of $U_{1-x}Gd_xO_{2-y}$ in 2 mol.L^{-1} HNO_3 at 60°C.

DISSOLUTION OF (U,GD)O_2 SINTERED SAMPLES : IMPACT OF THE SYNTHESIS ROUTE

In order to demonstrate the possible impact of the synthesis route of solid solutions on their chemical durability, dissolution tests were carried out on two pellets of $U_{0.80}Gd_{0.20}O_2$, the first being prepared from hydroxide and the second from oxalate precursor. The evolution of the

This project has received funding from the EURATOM research and training programme 2017-2021 under grant agreement No 755171

relative mass losses during the dissolution of both samples in 2 mol.L^{-1} HNO_3 at 60°C are gathered in **Figure 19**.

The dissolution kinetics were found to be very close for the two samples. Indeed, even if the elemental release in solution seemed to be faster during the induction period for the sample prepared by the hydroxide route (4% of dissolution after 6 hours compared to only 1% for the pellet prepared from oxalate precursor), the full dissolution of both pellets was reached after 1 day. Thus, the synthetic route did not seem to impact the dissolution rate.

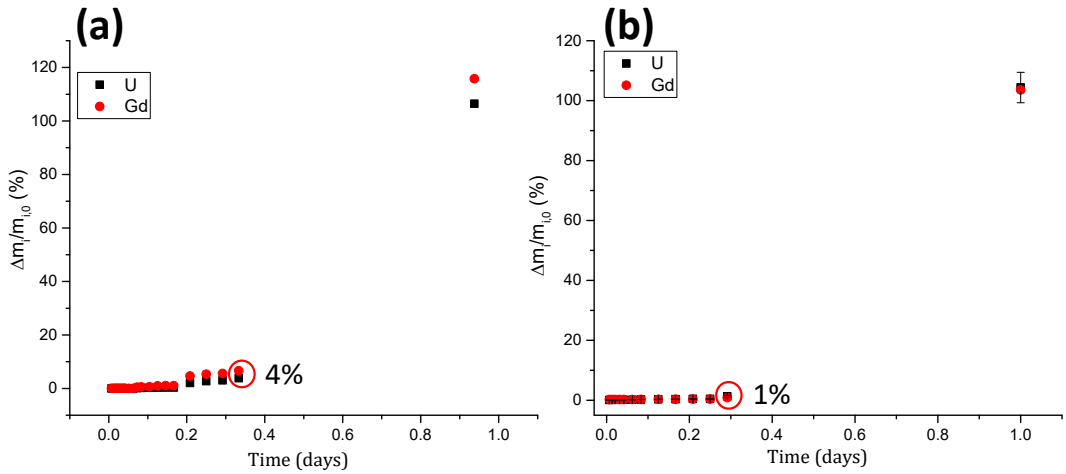

Figure 19. Evolution of the relative mass losses during the dissolution in 2 mol.L^{-1} HNO_3 at 60°C of sintered samples of $U_{0.80}Gd_{0.20}O_2$ obtained by hydroxide route (a) and by oxalic route (b).

DISSOLUTION OF SINTERED SAMPLES: COMPARISON BETWEEN (U,GD)O_2 AND (U,ND)O_2 SOLID SOLUTIONS

The aim of this paragraph is to check that the nature of the trivalent lanthanide does not affect the chemical durability of the final sintered pellets during dissolution tests. With this aim, sintered samples were prepared by the hydroxide route and then sintered at 1600°C for 4 hours under Ar-H_2. Both samples exhibited a densification rate close to 90%. The evolution of the relative mass losses obtained during the dissolution of sintered samples of $U_{0.80}Gd_{0.20}O_2$ (a) and $U_{0.80}Nd_{0.20}O_2$ (b) in 2 mol.L^{-1} HNO_3 at 60°C are reported in **Figure 20**.

As it was expected, the nature of the lanthanide element did not impact significantly the dissolution kinetics, with the complete dissolution of both sintered samples within 1 day. However, a longer induction period was noted for $U_{0.80}Gd_{0.20}O_2$ in comparison to $U_{0.80}Nd_{0.20}O_2$. This observation was already observed during the dissolution of powdered samples.

This project has received funding from the EURATOM research and training programme 2017-2021 under grant agreement No 755171

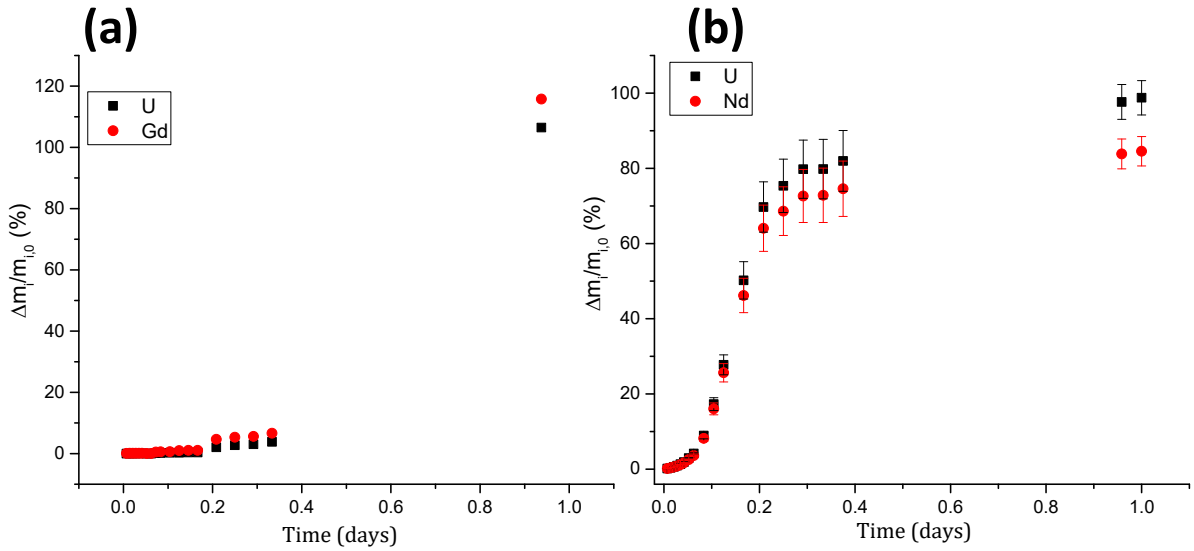

Figure 20. Evolution of the relative mass losses during the dissolution of sintered samples of $U_{0.80}Gd_{0.20}O_2$ (a) and $U_{0.80}Nd_{0.20}O_2$ (b) in 2 mol.L^{-1} HNO_3 at 60°C.

DISSOLUTION OF $(U,GD)O_2$ AND $(U,ND)O_2$ SINTERED SAMPLES: IMPACT OF THE LANTHANIDE MOLE LOADING

The evolution of the relative mass losses during the dissolution in 2 mol.L^{-1} HNO_3 at 60°C of various $(U,Gd)O_2$ and $(U,Nd)O_2$ sintered pellets with various lanthanide mole loadings are reported in **Figure 21**.

Whatever the nature of the lanthanide element, for loading rates lower than 20%, the dissolution kinetics of the pellets were almost the same. This result appears in good agreement with the previous results, showing that the kinetics of the solid solutions with large uranium contents was controlled by uranium (IV) oxidation. However, we already reported the particular behavior of the neodymium bearing samples, with a much shorter induction period (step 2) than for samples containing gadolinium. Regarding to the latter materials, the normalized dissolution rate reached almost 100 g.m^{-2}.d^{-1}, which was in good agreement with the data obtained on powdered samples. Also, it should be noted that the samples containing 50 mol.% of gadolinium exhibited no clear induction period, which was explained by the high trivalent lanthanide content and the associated weakening of the energy of cohesion of the crystal structure. Additionally, the rate of dissolution associated to the catalyzed period (step 3) was slower due to the lower uranium contents in the samples (this element being oxidized during dissolution in nitric acid). Once again, this result agrees well with that observed on powdered materials.

This project has received funding from the EURATOM research and training programme 2017-2021 under grant agreement No 755171

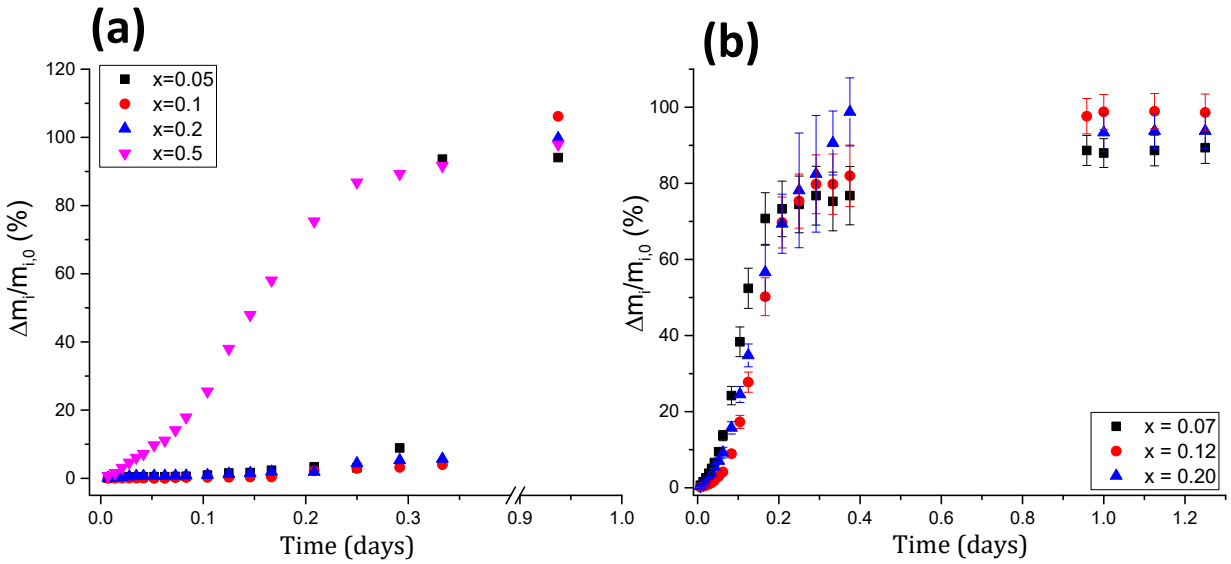

Figure 21. Evolution of the relative mass losses obtained during the dissolution in 2 mol.L^{-1} HNO_3 and at 60°C of several $U_{1-x}Gd_xO_2$ (a) and $U_{1-x}Nd_xO_2$ (b) sintered pellets with various lanthanide mole loadings.

OPERANDO MONITORING OF THE SOLID/LIQUID INTERFACE DURING THE DISSOLUTION OF (U,ND)O2 AND (U,GD)O2 SINTERED PELLETS BY ESEM : MICROSOCPIC APPROACH

As it has been done for $(U,Ce)O_2$ solid solutions, operando monitoring by ESEM of the evolving solid/liquid interface was developed for $(U, Nd)O_2$ and $(U, Gd)O_2$ pellets during dissolution tests in 2 mol L^{-1} HNO_3 and at 60°C. In order to follow the degradation of the sample microstructure, several zones were selected at the surface of the materials then followed versus time (i.e. for different progresses of the dissolution reaction). The series of micrographs are gathered in **Figure 22** and in **Figure 23** for the $U_{0.80}Gd_{0.20}O_2$ and the $U_{0.80}Nd_{0.20}O_2$ pellets, respectively. The dissolution time as well as the associated relative mass loss are indicated in each micrograph.

This project has received funding from the EURATOM research and training programme 2017-2021 under grant agreement No 755171

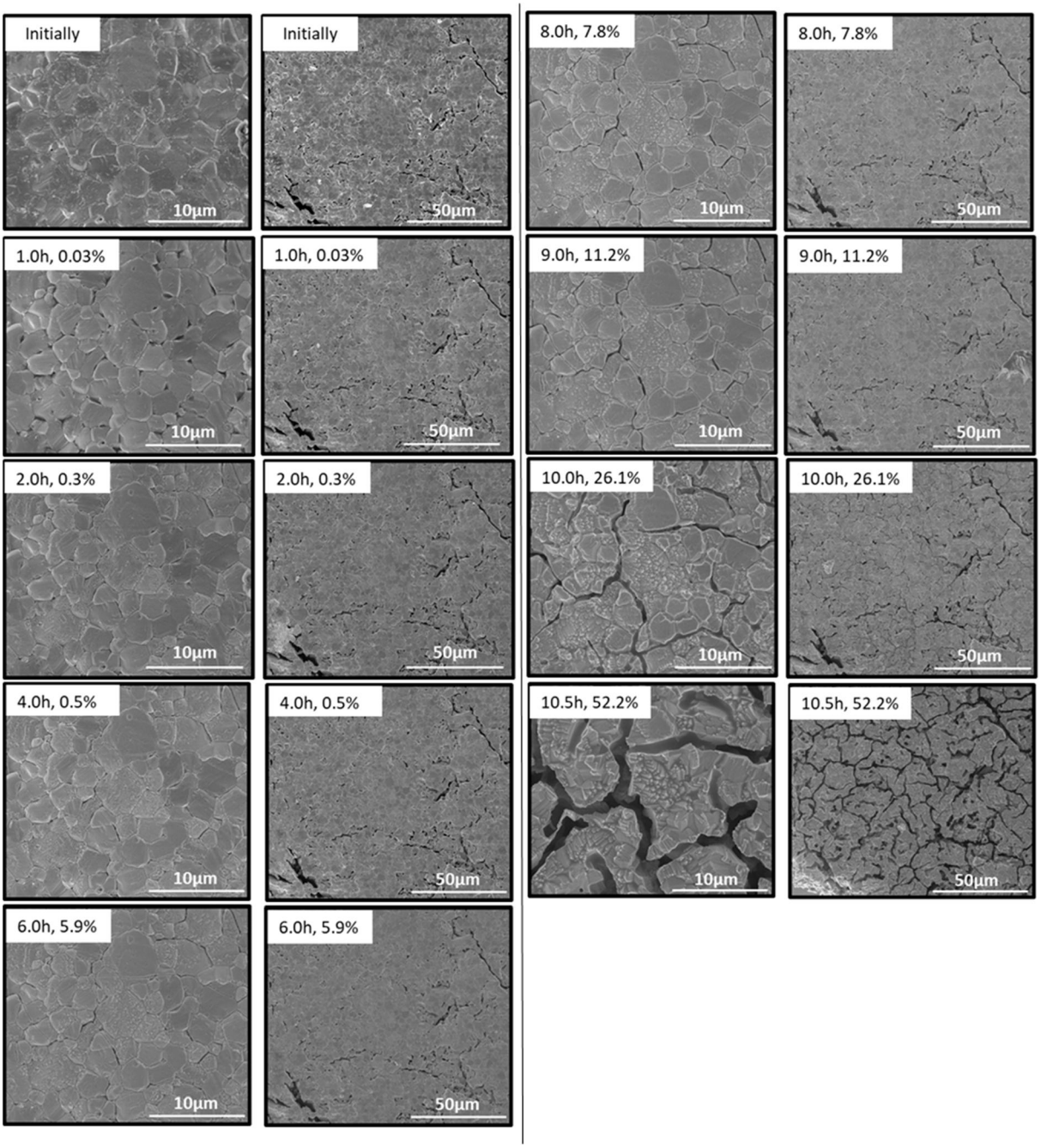

Figure 22. Operando monitoring of the solid/liquid interface by ESEM recorded during the dissolution of sintered pellet of $U_{0.80}Gd_{0.20}O_2$ in 2 mol L^{-1} HNO_3 at 60°C (two different magnifications).

This project has received funding from the EURATOM research and training programme 2017-2021 under grant agreement No 755171

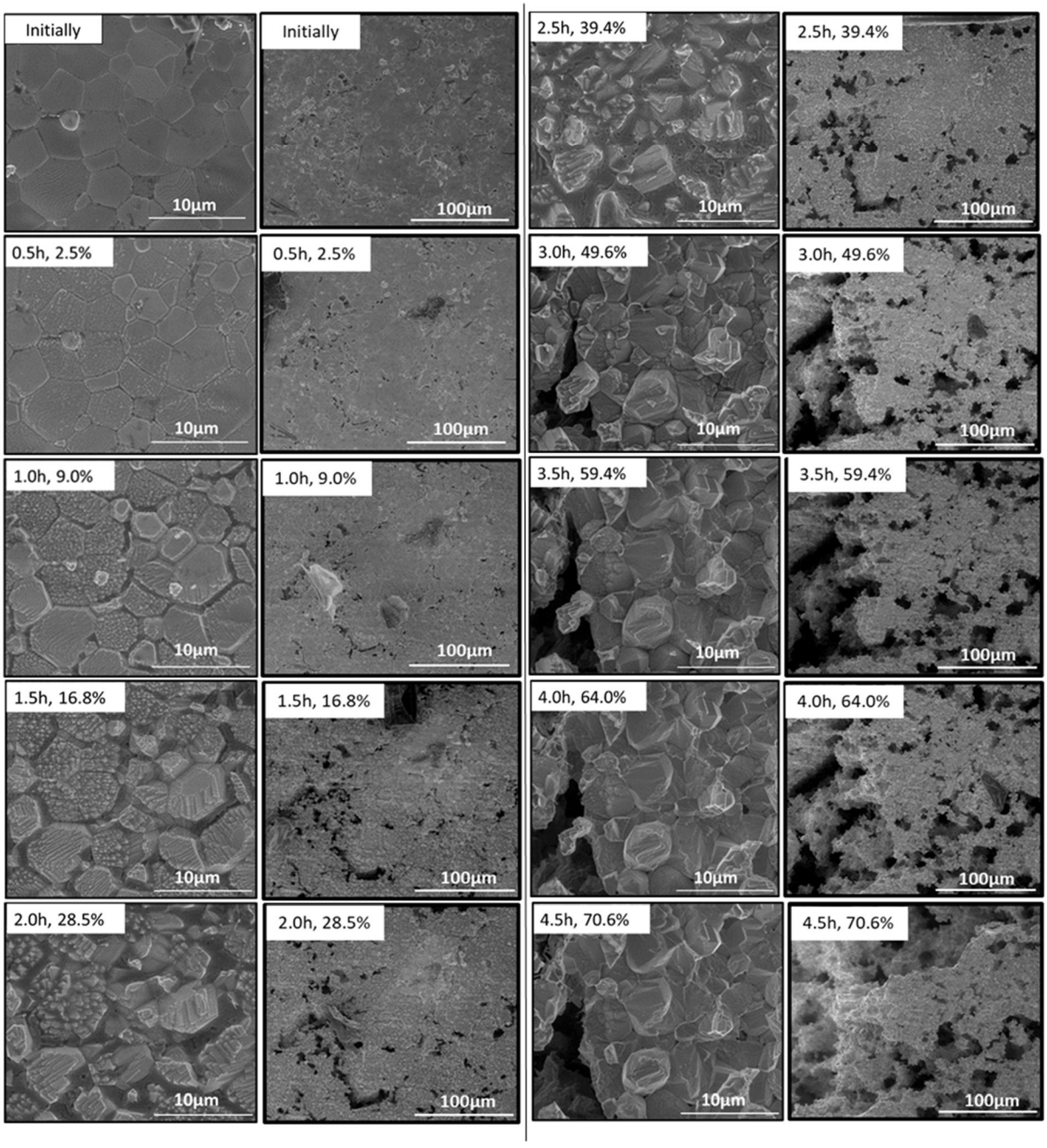

Figure 23. Operando monitoring of the solid/liquid interface by ESEM recorded during the dissolution of sintered pellet of $U_{0.80}Nd_{0.20}O_2$ in 2 mol L^{-1} HNO_3 at 60°C (two different magnifications).

This project has received funding from the EURATOM research and training programme 2017-2021 under grant agreement No 755171

Whatever the sintered sample considered, the evolution of the surface involved three successive stages:

- First, the preferential dissolution of the grain boundaries was observed (up to approx. 10 wt.% of dissolution progress), surely due to their slight enrichment in lanthanide elements (which could act as a local weakness at the surface of the solids) ;
- It was followed by the dissolution of the grains themselves. This step was clearly associated to the formation of the different dissolution features associated with the crystal orientation of the grains. According to the recent works of Bertolotto et al. on UO_2, the observation of square pyramids with comparable size and all aligned along the same direction is linked to the dissolution of the oriented (100) surface. On the contrary, the “chevrons” formed at the solid/liquid interface are associated to the dissolution of the (110) orientation whereas the triangular corrosion pits are linked to the (111) oriented surface [7]. It induces different local progresses of the dissolution depending on the grains orientation.
- The third and last step was connected to the establishment of the catalyzed period. The phenomena were more easily observed for the smallest magnifications with the development of large porosity in the pellet. This digging had a significant impact on the increase of the developed surface (thus of the sample reactivity) at the solid/liquid interface. It was surely responsible for the accumulation of nitrous acid within the pores (acting as confined domain where the progress of the dissolution reaction could be significantly increased).

The comparison of both gadolinium based and neodymium based solid solutions confirmed the differences observed at the macroscopic level. Right now, no clear explanation can be formulated. Strong differences are not expected between both lanthanide elements either in solution or in the fluorine structure. One could imagine some differences coming from the last step of the material preparation, i.e. the sintering step. Complementary experiments are now under progress to study this particular point.

CONCLUSIONS

In order to study the dissolution of uranium -lanthanide oxide solid solutions, complementary routes of preparation of precursors have been developed to prepare a large panel of solid solutions (deliverable D 4.4.). Several types of powdered and sintered samples were submitted to various dissolution tests and then the impact of several parameters of interest were evidenced.

For homogeneous $(U,Ce)O_2$ samples, uranium and cerium were released almost congruently during all the dissolution tests. Moreover, at room temperature, the evolution of all the normalized mass losses exhibited a two-steps evolution. The first one (not-catalyzed domain) was mainly associated to surface driving reactions. During the second step (catalyzed domain), the evolutions of the standardized mass losses then became non linear and corresponded to the fast release of the cations in the solution. At room temperature, the normalized dissolution rates obtained for uranium-lanthanide solid solutions were found to be

This project has received funding from the EURATOM research and training programme 2017-2021 under grant agreement No 755171

higher than for the pure end members. Almost no variation versus the chemical composition was noted for $0.1 \leq x \leq 0.5$ then a decrease of the normalized dissolution rate was observed for $x > 0.5$ (perhaps associated to the prevention of uranium (IV) from strong oxidation, due to large amounts of cerium in the materials). When making the dissolution tests at higher temperature (i.e. 60°C), the first step was not observed anymore (very short induction period observed). At this temperature, the dissolution of the materials remained congruent and was complete after less than 15 minutes, with a decrease of the normalized dissolution rates when incorporating lanthanide elements in the materials (possibly associated to the presence of uranium (V) in the samples).

In order to study the dissolution of $U_{1-x}Ce_xO_2$ solid solutions in the catalytic domain, the production of HNO_2 was followed in solution. It was found that, contrarily to pure UO_2, the concentration of nitrous acid was slightly lower than that of uranium, which could underline the potential consumption of HNO_2 by cerium (IV).

For heterogeneous sintered samples, the dissolution became uncongruent, with the preferential release of cerium compared to uranium, surely due to the presence of cerium (III) in the prepared pellets. Simultaneously, the chemical durability of the samples was decreased compared to that of homogeneous samples. Additionally, the duration of the induction period was shortened and then the samples were dissolved more rapidly.

Simultaneously to the macroscopic study, operando monitoring of the solid/liquid interfaces was performed for various sintered samples. The micrographs series suggested three stages in the pellet dissolution: grain boundaries first constituted preferential dissolution zones at the surface of the ceramics. With the progress of the dissolution reactions, several features characteristic of the grain orientations were evidenced. Finally, reaching catalyzed conditions induced the formation of large porosity within the pellets, in which the chemical reactions associated to the dissolution proceeded more rapidly.

This project has received funding from the EURATOM research and training programme 2017-2021 under grant agreement No 755171

LIST OF REFERENCES

[1] T. Cordara, S. Szenknect, L. Claparede, R. Podor, A. Mesbah, C. Lavalette, N. Dacheux, Kinetics of dissolution of UO_2 in nitric acid solutions: A multiparametric study of the non-catalysed reaction, J. Nucl. Mater. 496 (2017) 251-264.

[2] T. Dalger, S. Szenknect, F. Tocino, L. Claparede, A. Mesbah, P. Moisy, N. Dacheux, Kinetics of dissolution of $Th_{0.25}U_{0.75}O_2$ sintered pellets in various acidic conditions, J. Nucl. Mater. 510 (2018) 109-122.

[3] D. Horlait, N. Clavier, S. Szenknect, N. Dacheux, V. Dubois, Dissolution of Cerium(IV)-Lanthanide(III) Oxides: Comparative Effect of Chemical Composition, Temperature, and Acidity, Inorganic Chemistry 51(6) (2012) 3868-3878.

[4] L. Claparede, N. Clavier, N. Dacheux, P. Moisy, R. Podor, J. Ravaux, Influence of Crystallization State and Microstructure on the Chemical Durability of Cerium-Neodymium Mixed Oxides, Inorganic Chemistry 50(18) (2011) 9059-9072.

[5] D.Horlait, F.Tocino, N.Clavier, N.Dacheux, S.Szenknect, Multiparametric study of $Th_{1-x}Ln_xO_{2-x/2}$ mixed oxides dissolution in nitric acid media, Journal of Nuclear Materials, 429, Issues 1–3, (2012) 237-244.

[6] F. Tocino, Contrôle Microstructural Des Réactions Rédox à l'interface Solide/Solution Lors de La Dissolution d'oxydes Mixtes à Base d'uranium (+IV), Université de Montpellier, 2015

[7] S. Bertolotto, S. Szenknect, S. Lallema, A. Magnaldo, P. Raison, M. Odorico, R. Podor, L. Claparede, N. Dacheux, Effect of surface orientation on dissolution rate and surface dynamics of UO_2 single crystals in nitric acid, Corrosion Science 176 (2020) 109020.

[8] J. Martinez, N. Clavier, A. Mesbah, F. Audubert, X.F. Le Goff, N. Vigier, N. Dacheux, An original precipitation route toward the preparation and the sintering of highly reactive uranium cerium dioxide powders, Journal of Nuclear Materials, 462 (2015) 173-181.

[9] N. Clavier, Y. Cherkaski, J. Martinez, S. Costis, T. Cordara, F. Audubert, L. Brissonneau, N. Dacheux, Synthesis and direct sintering of nanosized $(M^{IV},M^{III})O_{2-x}$ hydrated oxides as electrolyte ceramics, Chem. Phys. Chem., 18 (2017) 2666-2674.

This project has received funding from the EURATOM research and training programme 2017-2021 under grant agreement No 755171